



A trial of in situ and static measurements of levels of radioactive cesium 137 on shallow rugged reefs lying close to the coastline of Fukushima[☆]

Fumie Suzuki^{a,b,*}, Hideo Ohashi^{a,b}, Hiromi Shibata^{a,c}, Ken-ichi Nogami^a, Hisayuki Arakawa^b, Nobuhiro Shiotani^a

^a EcoStudies Association, Toranomon 2-2-5, Minato, Tokyo 105-0001, Japan

^b Tokyo University of Marine Science and Technology, Minato, Tokyo 108-8477, Japan

^c The Institute of Scientific and Industrial Research, Osaka University, Ibaraki, Osaka 567-0047, Japan

ARTICLE INFO

Keywords:

¹³⁷Cs
⁴⁰K
 Level
 In situ and static technique
 Reefs
 Fukushima Daiichi Nuclear Power Plant

ABSTRACT

With the use of an in situ and static method for gamma-ray measurements, levels of radioactive cesium 137 on shallow rugged reefs which lie between 37.3° N and 37.4° N, from the coastline of Fukushima to 141.06° E, at a depth of around 10 m were surveyed for the first time from May 2016 to December 2017. To confirm the contact between the detector and a surface of rock, we used a fact that potassium containing minerals are abundant and uniformly distributed in the area, and thus the strength of the photoelectric peak of natural radioactive potassium 40 is nearly constant over the area. We have found that the levels of radioactive cesium 137 varied from point to point within a range from 1×10^4 Bq/m² to 6×10^4 Bq/m².

1. Introduction

On March 11th, 2011, the Great East Japan Earthquake and subsequent tsunami hit the Fukushima Daiichi Nuclear Power Plant (FDNPP) of the Tokyo Electric Power Company. Consequently a vast amount of radioactive materials were released into the atmosphere from the three crippled nuclear reactors (Gov. Jpn., 2011; IAEA, 2011). In addition to the atmospheric fallout, the heavily contaminated cooling water directly discharged into the ocean (e.g., Tsumune et al., 2012; and the references therein). Less contaminated groundwater and river inflows were also the sources of contamination of the ocean.

To obtain a reliable estimate of the source terms, Science Council of Japan (2014) conducted a comprehensible comparison of the simulation results of nine regional atmospheric models, six global models, and eleven oceanic models for the transportation and deposition of radioactive materials. A review article by Buessler et al. (2017) summarized the results of the estimates of the source term for radioactive cesium 137 (¹³⁷Cs, T_{1/2} = 30.17 years) obtained from 19 different models reported until 2016. The estimates of the total atmospheric fallout of ¹³⁷Cs range from 8.8 PBq (Terada et al., 2012) to 50 PBq (Stohl et al., 2012), those of the fallout only over the ocean range from 5 PBq (Kawamura et al., 2011) to 14.8 PBq (Aoyama et al., 2016), and the

total amount of the direct discharges of ¹³⁷Cs to the ocean ranges from 3.5 PBq (Kobayashi et al., 2013) to 26.9 PBq (Bailey du Bois et al., 2012). The estimated values vary greatly because of uncertainty in the transportation and deposition processes and the insufficiency of measured data to carry out inverse calculations.

On land, the measurements of distribution and level of contamination with radioactive cesium 134 (¹³⁴Cs, T_{1/2} = 2.06 years) and ¹³⁷Cs were started immediately after the accidents. The results are compiled and made open to the public by the Nuclear Regulation Authority, Japan (NRA) on their website (NRA, 2018). On the seafloor of the coastal ocean, however, the measurements have been limited because of many technical difficulties. Using a sampling technique Kusakabe et al. (2013, 2017) surveyed the distributions and levels of ¹³⁷Cs and some other radioactive nuclides in the sediments which were sampled at 35 points on the seafloor of the continental shelf off Fukushima, between 35.5° N and 39.0° N, and between the coastline and 142° E, excluding an area within a radius of 30 km from the FDNPP. Also using the sampling technique, Black and Buessler (2014) collected twenty sediment cores in a wide area between 36.5° N and 38.5° N, and between the coastline and 143.5° E. Ambe et al. (2014) collected sediments samples at 113 points with a regular interval of 5 min of latitude and longitude in an area between 36.5° N and 37.8° N, and between the

[☆] This research did not receive any specific grant from funding agencies in the public, commercial, or not-for-profit sectors.

* Corresponding author at: EcoStudies Association, Toranomon 2-2-5, Minato, Tokyo 105-0001, Japan.

E-mail addresses: suzuki@ecostudies.jp (F. Suzuki), ohashi@ecostudies.jp (H. Ohashi), shibata@ecostudies.jp (H. Shibata), nogami@ecostudies.jp (K.-i. Nogami), arakawa@kaiyodai.ac.jp (H. Arakawa), shiotani@ecostudies.jp (N. Shiotani).

<https://doi.org/10.1016/j.marpolbul.2019.06.007>

Received 23 November 2018; Received in revised form 8 April 2019; Accepted 3 June 2019

0025-326X/© 2019 Elsevier Ltd. All rights reserved.

coastline and 141.5° E, excluding an area within a radius of 20 km from the FDNPP. Thornton et al. (2013a, 2013b) developed a towed gamma-ray spectrometer of a standard combination of a NaI(Tl) scintillator and a photomultiplier tube and carried out in situ and continuous measurements to study the distribution of ^{137}Cs on the seafloor of a rectangular area, from 37°20' N to 37°30' N and from 141°03' E to 141°15' E. They have revealed the existence of local anomalies as high as 40,000 Bq/kg-wet in the levels of ^{137}Cs . Then, the NRA (2014, 2015, 2016, 2017) commissioned the projects for continuation of the studies on the above mentioned rectangular area with the use of the towed gamma-ray spectrometer, the sampling technique and the on-land analyses of sediments. The results have revealed that the average level of ^{137}Cs on the soft seafloor is a few hundred Bq/kg-wet. The technique of towing the gamma-ray spectrometer has been particularly useful to map the continuous distribution of ^{137}Cs on the soft seafloor with a gentle undulation.

Regarding the survey of contamination on shallow rugged reefs which lie between the coastline and 141.06° E, to the best of the authors' knowledge, no systematic survey has been reported. Obviously, the sampling technique cannot be employed to study hard bottoms unless a practical technique for scraping surfaces of rock is available. Very recently Matsumoto et al. (2018) employed an air-lift method successfully to collect sediments on rock on the shallow seafloor. The air-lift method, however, may not yield full information about the level of ^{137}Cs on rock because not all the sediments on a rock surface can be air-lifted. The only practical method that is applicable to survey the contamination on the shallow rugged reefs near the FDNPP is an in situ and static method. It should be noted that shallow rugged reefs lie along the coastline of Fukushima before the continental shelf of sandy seafloor starts. The data of the current status of contamination on the shallow rugged reefs to which heavily contaminated cooling water was directly spewed would be indispensable to refine various oceanic simulation models for transportation and deposition of radioactive materials.

The aim of this study is to report the levels of radioactive cesium on the shallow rugged reefs which lie between 37.3° N and 37.4° N, and between the coastline of Fukushima and 141.05° E.

In Section 2 the present in situ and static method is briefly explained, and data processing is described. In Section 3 the results are presented, and the uncertainties involved in the data are discussed. The conclusion is given in the last section.

2. Experimental

2.1. Instrumentation

A scintillator is used as a gamma-ray detector. The reason is that an estimated level of contamination with ^{137}Cs is in order of 10^4 Bq/m², and we do not intend to study various reactor-made radioactive nuclides by measuring energies of photoelectric peaks with an energy resolution that only a pure Ge detector can provide. Instead of choosing a standard combination of NaI(Tl) scintillator and photomultiplier tube (PMT), we have employed a combination of CsI(Tl) scintillator and photodiode. A detailed comparison of characteristics between the former and the latter is given in a recent review by Belousov et al. (2017). The main reason why we chose the combination of CsI(Tl) and photodiode is that it has a great advantage over a NaI(Tl) scintillator with a PMT in regard to compactness, low-deliquescence and mechanical strength, such as potential damage due to impact with rock and due to handling on board of a fishing boat.

The detector employed in the present survey is a gamma-ray spectrometer KESVM1 made to order by Kansai Electronics Co., Ltd., Japan. The spectrometer consists of a CsI(Tl) cylindrical crystal of 25.4 mm in diameter and 25.4 mm in height and Si PIN photodiode S6775 made by Hamamatsu Photonics K.K., Japan. The specifications are summarized in Table 1. Together with the CsI(Tl) crystal with photodiode, the signal

processing circuit, A/D converter, 4096 channel multichannel analyzer, a central processing unit and a Universal Serial Bus (USB) interface are housed in a compact aluminum case. Then, the case is contained in a pressure tight vessel (PTV), the dimensions of which are described in Table 1. The data are forwarded to a personal computer on a boat by a USB cable of 50 m in length which has three repeaters.

The detection efficiency of the detector was measured by a standard method using a point source of ^{137}Cs manufactured by Amersham, the source code of which is CDR8. The strength was calibrated to be 2.604×10^6 Bq on February 17th, 2012 by Japan Radioisotope Association. In actual measurements, however, the PTV contacts a contaminated surface of rock which can be regarded as a two-dimensionally extended source. To take into account the effects of this extended nature in determining a factor to convert the count rate to the amount of ^{137}Cs seen by the detector, we simulated the situation by putting the detector in the PTV on a rectangular plate source of ^{137}Cs manufactured and calibrated by Japan Radioisotope Association, the source code of which is CS221. The source had a density of 1×10^4 Bq/m² on December 1st, 2011. The size of the plate was 100 mm × 100 mm and was large enough compared with the diameter of the CsI(Tl) crystal. Fig. 1 shows a raw spectrum of the plate source of ^{137}Cs measured in our laboratory. The measurement time was 600 s. In addition to the photoelectric peak of ^{137}Cs , a weak but discernible photoelectric peak of radioactive potassium 40 (^{40}K , $T_{1/2} = 1.25 \times 10^9$ years) is recorded, which originates from the concrete walls, floor and ceiling of the laboratory. A raw spectrum of the background in the lab is shown in Fig. S1 which is in the Supplemental Data. In Fig. 2 is shown the photoelectric peak fitted with a Gaussian function after subtraction of a baseline (see Section 2.3). The full width at half maximum (FWHM) of the photoelectric peak gives the energy resolution at 662 keV to be 9.0%. Similarly, the energy resolution of the detector at 1462 keV is determined to be 5.9% from the FWHM of the photoelectric peak of ^{40}K in Fig. S1 in the Supplementary data. From the total counts under the photoelectric peak of ^{137}Cs , the factor to convert the count rate in counts per second (cps) to the amount of ^{137}Cs seen by the detector is obtained to be one cps equal to 6.32×10^4 Bq/m². Separation between the photoelectric peak of ^{137}Cs at 662 keV and that of ^{134}Cs at 796 keV is seen in Fig. SR1 which is in the Supplementary data.

A cage was made to accommodate the detector in the PTV and various auxiliary sensors such as an underwater pressure sensor (MS5837-30BA, Measurement Specialties, Inc., CA, USA) to know the depth and an attitude sensor (MPU-9250, Strawberry Linux Co., Ltd., Tokyo, Japan) to know how stable the cage stands on the hard seafloor. A schematic drawing is shown in Fig. SR2 which is in the Supplementary data.

The USB signal cable, the power supply line, the video signal cables, and the signal lines from the sensors were bundled together. The cage is tied to the end of the rope by three chains from the frame of the cage. Independently the PTV is tied to the same end of the rope by three wires. To protect the thin window for gamma rays on the bottom of the PTV on landing upon hard seafloor, the length of the wires are adjusted in a way that the bottom of the PTV is 50 mm above the bottom of the cage so that the PTV never lands on a rock surface before the cage lands. Another little ingenuity is exercised. After the cage lands, we let the rope go out farther by about 10 m to settle the end of the rope on the top of the cage. Then the PTV can freely go through the hard vinyl chloride pipe fatter down by about 40 mm from the bottom of the cage. In this way, even when a gap between the central part of the bottom of the cage and the surface of rock is created by landing of the bottom frame of the cage on two or three points which are protruded higher from the surface of rock, the PTV can slide down to contact the surface of rock.

Table 1
Specifications of gamma-ray spectrometer.

Scintillator	CsI(Tl) 25.4 mm in diameter and 25.4 mm in height
Opto-electric converter	Photo diode
Energy resolution	8.7% at 662 keV and 5.9% at 1462 keV
Detection efficiency	20% at 662 keV
Number of channels	4096
Energy range	70 keV–4 MeV
Pressure tight vessel (PTV)	Cylindrical aluminum case, 85 mm ϕ \times 240 mm, $t = 10$ mm. An area of 40 mm ϕ of the bottom of the case is thinned to 1 mm to serve as a window for incoming gamma-rays.

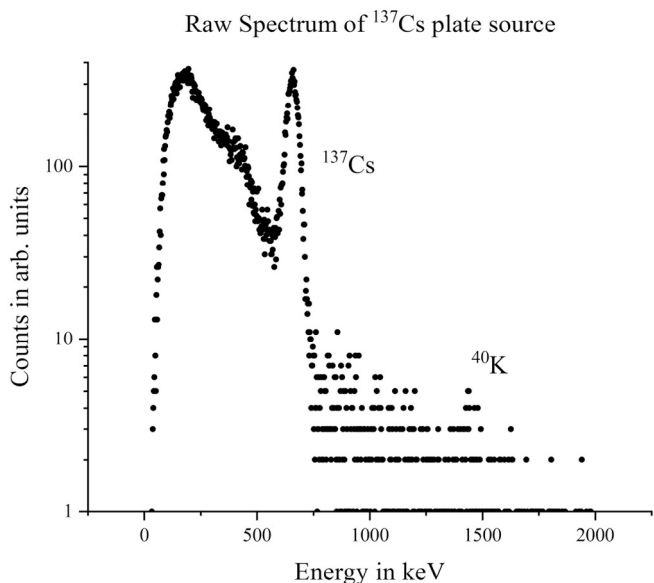


Fig. 1. Raw gamma-ray spectrum of the plate source of ^{137}Cs . The measurement time was 600 s. The photoelectric peak of ^{40}K is from the concrete of the wall, floor and ceiling of our laboratory.

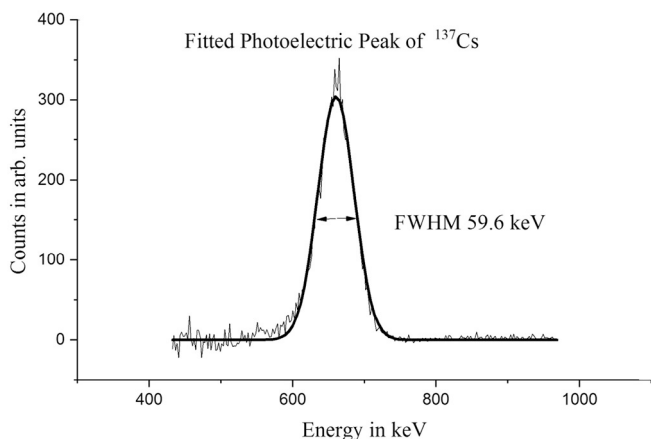


Fig. 2. Photoelectric peak of ^{137}Cs fitted with a Gaussian function. The photoelectric peak of ^{137}Cs shown in Fig. 1 was fitted with a Gaussian function after subtraction of the baseline (see Section 2.3). The data points are connected with thin straight lines. The full width at half maximum of the photoelectric peak gives an energy resolution at 662 keV to be 9.0%.

2.2. In situ and static method

Based on information about reefs obtained from Fukushima Prefectural Fisheries Experimental Station we selected those lying close to the coastline and near the FDNPP. Our fishing boat had an ultrasonic fish finder. From the degree of attenuation of the ultrasonic wave reflected at the bottom of the sea, we could confirm that the boat was

right above the reefs. The ultrasonic fish finder also gave a depth from a time for the ultrasonic wave to come back from the bottom of sea. The cage was lowered by a rope from the boat to the bottom of the reef and kept there for 1200 s to obtain a gamma-ray spectrum. In a typical operation for a depth of around 10 m, the time for lowering or raising the cage was just a few minutes. Since no time was used for the anchoring the boat in our study, each measurement was performed within 30 min. During the measurement, the live spectrum was being displayed on a monitor of a personal computer on the boat. From several preliminary measurements in the area, it was found that when the contact between the PTV and a surface of rock was not disturbed, the measurement time of 1200 s was just enough for the measured spectrum to have a discernible photoelectric peak of ^{40}K which could be subjected to an analysis to be described in Section 2.3.

The boat drifted naturally due to surface currents and winds. Therefore, while a gamma-ray spectrum was being taken, the rope and the bundle of the cables were kept slackened enough not to drag the cage. The position where the cage was lowered from the boat was marked on a GPS display of the boat so that the boat was continuously steered back to the initial position. The boat was not anchored. When a current at the bottom of the sea was strong, it pushed the bundle of the cables toward downstream and thus the cage was dragged in the same direction. In such case the bundle of the cables was anchored at the bottom so that the cage was not disturbed by the movement of the bundle of the cables. When a sudden and drastic change was found on the monitors of the video cameras and in the signal of the attitude sensor, the change was taken as an indication that the cage started to move or incline or be toppled over on its side by turbulent currents, and then the measurement had to be aborted.

2.3. Data processing

The reliability of the data is very much affected by the quality of the contact between the PTV and a surface of rock. If a gap between the bottom of the PTV and a surface of rock exists, the count rate must be less than that of the case with no gap. Using the X-ray mass attenuation coefficients for water given by Hubbell and Seltzer (1996), we can estimate that a gap of 20 mm filled with seawater would reduce the count rate of gamma-rays from ^{137}Cs by 16% and that of those from ^{40}K by 11%.

In actual measurements, it turned out that because of high turbidity, the images sent from the video cameras were almost always not clear and could not give information about a possible gap between the bottom of the PTV and a surface of rock. In this regard, our measurement seemed to be a sort of blind measurement. After examination of all the spectra, however, it was found that a weak but a well discernible photoelectric peak of ^{40}K was recorded in most of the spectra and its strength did not vary much from spectrum to spectrum, that is, the strength of ^{40}K is independent of the measured points and of the strength of the photoelectric peak of ^{137}Cs . All the raw spectra which have a well discernible photoelectric peak of ^{40}K are shown in Figs. S3–S20, and some of those which don't have are shown in Figs. S21–S24 which are in the Supplemental data. As an example, Fig. 3 shows a raw spectrum obtained at P01 on December 9th, 2017 the location of which is depicted in Fig. 4. We first focus our attention on the photoelectric

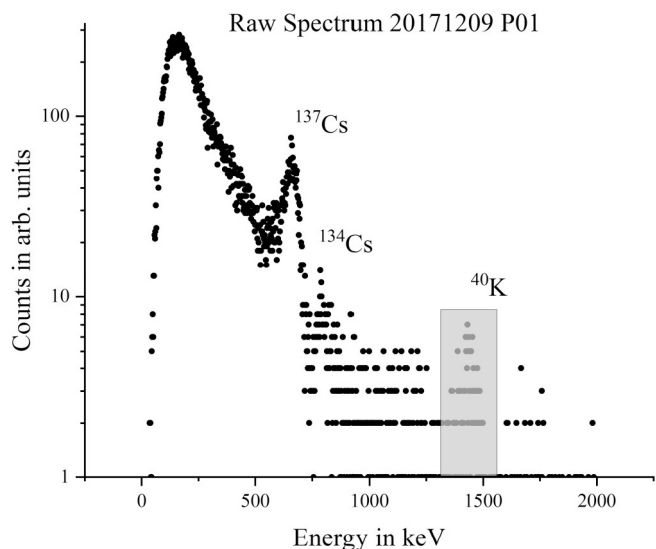


Fig. 3. Raw gamma-ray spectrum measured on Dec. 9, 2017 at P01. Photoelectric peak of ¹³⁷Cs at 662 keV is clearly observed and that of ¹³⁴Cs at 796 keV is discernible. Although weak, photoelectric peak of ⁴⁰K is also discernible in the shaded region, the width of which is $3\Gamma_{1462\text{keV}}$, where $\Gamma_{1462\text{keV}}$ is the energy resolution of the detector at 1462 keV. The location of P01 is shown in Fig. 4.

peak of ⁴⁰K in a shaded region with a width of $3\Gamma_{1462\text{keV}}$, where $\Gamma_{1462\text{keV}}$ is the FWHM of the photoelectric peak at 1462 keV. The present choice of the width of the shaded region is based on a fact that an integration of a Gaussian function with a standard deviation σ between -3σ and 3σ gives 99.7% of the total area under the function. The relation between the standard deviation and the FWHM is given by a relation, $\text{FWHM} = 2\sigma (2\ln 2)^{1/2}$. Thus, the present width of $3\Gamma_{1462\text{keV}}$ is a little wider than the width of 6σ .

According to the geochemical map published by Geological Survey of Japan (2003), the area we are interested in is located east of the Abukuma Mountains which consist mostly of granitic rock with abundant potassium. The natural radioactive potassium is, therefore, fairly evenly distributed on land and seafloor. Then, we can use the photoelectric peak of ⁴⁰K to quantify the contact. If the contact is attained, the count rate of the photoelectric peak of ⁴⁰K should be similar everywhere. On the basis of this consideration, all the raw spectra obtained were first inspected whether or not the photoelectric peak of ⁴⁰K was well discernible and could be fitted with a Gaussian function. Then, after discarding the spectra in which the photoelectric peak of ⁴⁰K was not found or vague, the total accumulated counts for a measurement time of 1200 s, N_K , in the shaded region in Fig. 3 were examined in every spectrum. The average value, $N_{K \text{ avg.}}$, was 129 counts. The values of N_K were found within a range of $N_{K \text{ avg.}} \pm 20$ counts. Although the number of accumulated counts in the shaded region was small and the scatter in N_K was a little larger than the statistical error, $(N_{K \text{ avg.}})^{1/2}$, the above fact indicated that the photoelectric peak of ⁴⁰K could be used to judge whether the bottom of the PTV contacted the hard bottoms or not. After these examinations, the spectra were subjected to analyses of the photoelectric peak of ¹³⁷Cs.

To extract information from the measured spectra, we used Origin Pro 2018 (Origin Lab Co. Northampton, MA, USA). Since the aim of the present survey was to know the amount of residual ¹³⁷Cs on the reefs, we examined the spectra in an energy range between 490 keV and 920 keV which covered 605 keV peak of ¹³⁴Cs, 662 keV peak of ¹³⁷Cs, and 796 keV peak of ¹³⁴Cs. First, the baseline was fitted with a B-spline curve. Then the three peaks were fitted with three Gaussian functions with a width which was obtained in the measurement of the resolution described in Section 2.1. The position of each peak was also fixed at that which was determined from the calibration of the channel-energy

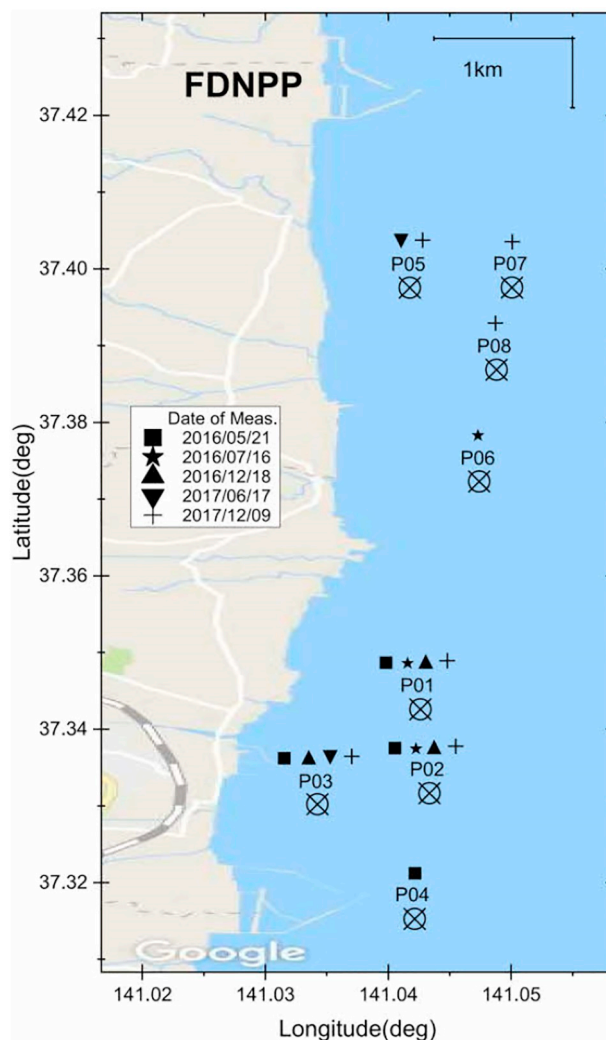


Fig. 4. The points at which the levels of ¹³⁷Cs were measured. The dates of measurements are indicated in the inset.

relation. Therefore, the actual fitting parameters were the heights of the three peaks. The statistical error was deduced from the number of counts under the fitted curve of 662 keV peak of ¹³⁷Cs. Because of the fixed time measurement of 1200 s the statistical error ranged from 2.5% to 5.8%. The plausibility of the fitting results was examined by taking a ratio of the total counts under 796 keV peak of ¹³⁴Cs to those under 662 keV peak of ¹³⁷Cs. The theoretical ratio was calculated from the half-life of ¹³⁴Cs and that of ¹³⁷Cs, the date of the measurements, and the number of gamma-rays emitted from 1 Bq of each nuclide with a widely accepted assumption that the ratio ¹³⁴Cs/¹³⁷Cs was very close to unity when they were spewed from the crippled nuclear reactors. Only qualitative comparison between theory and measurement could be made because the signal to noise ratio of the 796 keV peak of ¹³⁴Cs was not high enough to reliably quantify the total counts under the 796 keV peak of ¹³⁴Cs. For this reason, only the measured levels of ¹³⁷Cs in units of Bq/m² were determined from the count rate of the 662 keV peak of ¹³⁷Cs and the conversion factor described earlier in this section. The fitted results are shown in Fig. 5.

3. Results and discussion

The names of measured points, the dates of measurements, the GPS coordinates and the levels of residual ¹³⁷Cs in units of Bq/m² are listed in Table 2. The measurement time was 1200 s except for P01 measured on July 16th, 2016. The depth of all points was about 10 m. The

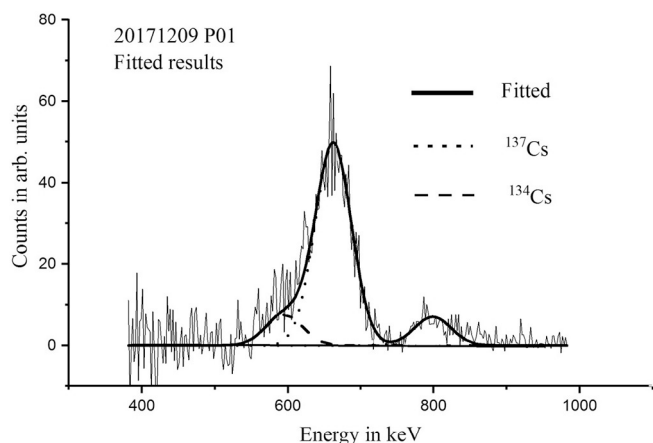


Fig. 5. The fitted results.

The photoelectric peaks of ^{137}Cs at 662 keV, those of ^{134}Cs at 605 keV, and at 796 keV shown in Fig. 3 are fitted with three Gaussian functions. The Gaussian curve centered at 796 keV (dashed line) is completely on top of the fitted curve (heavy line). As for the fitting procedure, refer to the text. The data points are connected with thin straight lines.

measured points are depicted in Fig. 4. All points were outside of the areas surveyed by Kusakabe et al. (2013, 2017), Black and Buessler (2014), Ambe et al. (2014), and Thornton et al. (2013a, 2013b).

Although the contact between the PTV and the hard seafloor is confirmed with recourse to the photoelectric peak of ^{40}K , there is still uncertainty involved in the measured levels. The video cameras could not show how firmly the bottom of the PTV was touching a surface of rock while the spectra were being taken. The readings of the attitude sensor were of some help to find out how stationary the cage was. The compass pointed to one direction most of the time, but sometimes the attitude sensor indicated that the inclination of the cage was intermittently changing in various directions. These facts suggested that turbulent currents swayed the cage and made a gap between the surface of rock and the bottom of the PTV open and closed. The sway caused reduction of the count rate. This may explain the fact that the fluctuation of N_K was a little larger than $(N_{K \text{ avg.}})^{1/2}$. Besides this, the cage was occasionally dragged by a current. Then, the measured value represents an average value along the trail. The overall uncertainty was estimated to be 16% to 17% by adding up the statistical error of the number of counts under the fitted 662 keV photoelectric peak of ^{137}Cs , which is 2.5% to 5.8%, and uncertainty in contact estimated from the fluctuation in N_K , which is 16%.

The measured levels of ^{137}Cs on the reefs range from $1 \times 10^4 \text{ Bq/m}^2$ to $6 \times 10^4 \text{ Bq/m}^2$. The values may be compared with that found by Thornton et al. (2013b) on the soft seafloor of sand, silt, clay or mixture of the three which extends toward east after the reefs we have surveyed. Although the original data of Thornton et al. (2013b) were given in units of Bq/kg-wet, later using the depth profiles of the concentration of ^{137}Cs obtained from analyses of the cores of sediments sampled independently, they have made it possible to convert the values in units of Bq/kg-wet to be in units of Bq/m^2 (NRA, 2016). The conversion leads to that, except the anomalously high levels found by Thornton et al. (2013b), the levels of ^{137}Cs at most of the points on the soft seafloor next to the reefs we have studied are in the order of 10^4 Bq/m^2 . The present levels on the reefs are in the same order of magnitude as those measured by Thornton et al. (2013b). Kusakabe et al. (2017) reported that the whole-core ^{137}Cs inventories at the monitoring points just outside of an arc of 30 km radius from the FDNPP ranged from $6 \times 10^3 \text{ Bq/m}^2$ to $8.5 \times 10^3 \text{ Bq/m}^2$ in October 2015, just about the same time as the present study was carried out.

Table 2 shows that the level of ^{137}Cs varies point by point and the temporal variation shows no apparent trend. Thornton et al. (2013b)

pointed out that the distribution was strongly influenced by meter scale features of the seafloor. Black and Buessler (2014) found that the level of ^{137}Cs varied even within one set of multicore samples collected simultaneously and immediately adjacent to one another. This fact must be kept in mind in looking at the data taken with a point by point method. In the present survey, the GPS coordinates are for the position of the boat, not for the cage on the reefs. While the cage is being lowered, the current pushes it downstream. Therefore, although the exact position of the cage will never be known, it is safe to say that the cage is within a radius of several meters from the GPS coordinates. A level of ^{137}Cs on a surface of rock may differ from that of another surface of the same rock. The large difference in the levels can be ascribed partly to the complexity of ruggedness of the reefs. Generally, surfaces of rock are not at all smooth. They are coarse, porous, with fine cracks and other irregularities in various scales which serve as trapping sites for contaminants to settle. Takahashi et al. (2017) showed that river waters in Fukushima were abundant with suspended particulates of several different types of phyllosilicate. Then, it is naturally expected that seawater along the coast of Fukushima is also abundant with suspended particulates of various types of phyllosilicate originated from the weathered granitic rock of the Abukuma Mountains. The phyllosilicate has pore or inter-layer space to be able to accommodate Cs ions in their own crystal structures (Nakao et al., 2014; Durrant et al., 2018). X-ray diffraction analyses of the sediments collected in the area where Thornton et al. (2013b) set show the existence of phyllosilicate such as illite, montmorillonite, and kaolinite (NRA, 2017). It has now become a widely accepted fact that once the atmospheric fallout is deposited on the surface of seawater or once the contaminated cooling water is spewed directly into seawater, a large part of radioactive cesium is trapped by these suspended particulates. Then, the fate of radioactive cesium is controlled by the fate of those particulates in seawater. Being subjected to transportation, dispersion and deposition mechanisms in seawater, the contaminated particulates reach surfaces of rock and are trapped either firmly or loosely depending on the irregularities of the surface of rock. Occasionally, when the cage hit a surface of rock, a rise of a thin cloud of sediments could actually be seen on the monitor of the video camera. The particulates trapped loosely may contribute to the temporal variations.

To reduce the uncertainties involved in the present in situ and static method, since uniform distribution of ^{40}K is not absolutely guaranteed by an independent geochemical survey of the bottom of the sea in the region with a much finer mesh than the one we cited, in addition to measuring ^{40}K , it is necessary to have some sort of device to directly confirm the contact between the detector and surfaces of rock. Also, it is desirable to use a CsI(Tl) scintillator larger in volume to increase the number of counts in the photoelectric peaks of ^{40}K and ^{137}Cs in a limited measurement time.

4. Conclusion

With the use of an in situ and stand still method and with recourse to the photoelectric peak of naturally coexisting ^{40}K , the levels of ^{137}Cs on the shallow rugged reefs which lie between 37.3° N and 37.4° N , and from the coastline of Fukushima to 141.06° E , at a depth of around 10 m were surveyed for the first time from May 2016 to December 2017. The levels varied from point to point within a range from $1 \times 10^4 \text{ Bq/m}^2$ to $6 \times 10^4 \text{ Bq/m}^2$ with an overall accuracy of 16–17%. The levels also changed with the dates of the measurement, but no apparent trend was found in the temporal variations. Considering the time needed to obtain a gamma-ray spectrum with statistics high enough to analyze the photoelectric peak of ^{137}Cs by curve fitting with a Gaussian function, we have found that the present apparatus is practical only in situations where the level of ^{137}Cs is higher than $1 \times 10^4 \text{ Bq/m}^2$.

Supplementary data to this article can be found online at <https://doi.org/10.1016/j.marpolbul.2019.06.007>.

Table 2

Names of the points, dates of measurements, GPS coordinates of the points and levels of residual ^{137}Cs in units of Bq/m^2 .

The depth of all points is about 10 m. All the level values are not decay corrected. The overall uncertainty of the levels is estimated to be 16–17%. Regarding the uncertainty, refer to the text.

Date of measurements (yyyy/mm/dd)		2016/05/21	2016/07/16	2017/06/17	2017/12/09
Name of measured point		P01			
GPS coordinates	N [deg]	37.3416	37.3426	37.3425	37.3428
	E [deg]	141.0398	141.0399	141.0399	141.0398
Measurement time	[s]	1200	627	1200	1200
Level of ^{137}Cs	10^4 [Bq/m^2]	2.7	2.2	2.5	6.1
Date of measurements (yyyy/mm/dd)		2016/05/21	2016/07/16	2017/06/17	2017/12/09
Name of measured point		P02			
GPS coordinates	N [deg]	37.3317	37.3317	37.3317	37.3313
	E [deg]	141.0434	141.0434	141.0433	141.0434
Measurement time	[s]	1200	1200	1200	1200
Levels of ^{137}Cs	10^4 [Bq/m^2]	2.7	1.4	1.5	0.6
Date of measurements (yyyy/mm/dd)		2016/05/21	2016/12/18	2017/06/17	2017/12/09
Name of measured point		P03			
GPS coordinates	N [deg]	37.3302	37.3299	37.3301	37.3301
	E [deg]	141.0342	141.0344	141.0342	141.0340
Measurement time	[s]	1200	1200	1200	1200
Levels of ^{137}Cs	10^4 [Bq/m^2]	2.3	1.4	2.7	5.3
Date of measurements (yyyy/mm/dd)		2016/05/21		2017/06/17	2017/12/09
Name of measured point		P04		P05	
GPS coordinates	N [deg]	37.3152		37.3976	37.3973
	E [deg]	141.0423		141.0418	141.0420
Measurement time	[s]	1200		1200	1200
Level of ^{137}Cs	10^4 [Bq/m^2]	2.8		3.5	2.2
Date of measurements (yyyy/mm/dd)		2016/07/16		2017/12/09	2017/12/09
Name of measured point		P06		P07	P08
GPS coordinates	N [deg min]	37.3701		37.3976	37.3868
	E [deg min]	141.0468		141.0500	141.0487
Measurement time	[s]	1200		1200	1200
Level of ^{137}Cs	10^4 [Bq/m^2]	4.2		2.6	2.0

Author contributions

F. Suzuki, H. Ohashi, H. Arakawa and N. Shiotani planned and designed the project.

H. Ohashi and F. Suzuki organized and supervised the works onboard.

F. Suzuki and N. Shioatani were in charge of acquisition of the radiation data onboard.

H. Shibata and K. Nogami were in charge of acquisition of the data from the video cameras and the attitude sensor onboard.

N. Shiotani, H. Suzuki, and H. Ohashi processed the data and prepared the manuscript.

All the authors discussed the results and read critically the manuscript.

Declaration of Competing Interest

The authors declare that they have no competing interests.

Acknowledgments

The authors thank S. Tomihara for providing precious information about the present status of the sea off Fukushima. We also thank Iwaki Fishery Cooperative for understanding the aim of our survey and for introducing us to Captain Ishii and his fishing boat Choeimaru. We greatly appreciate Captain Ishii's knowledge of the reefs and his skill to keep his boat at a designated point against winds and currents. We express our gratitude to T. Kobayashi, K. Umeda and H. Akai for illuminating discussions. Without generous supports from A. Okada, N. Kumagai, K. Ito, Y. Yamada, K. Sato, J. Yamada, K. Shinji, Y. Yamazaki, A. Koga, K. Murooka, H. Fujibayashi, M. Tsuchida, and E. Shinoda, this research project would not have been materialized. One of the authors (HO) would like to thank the technical staff members of the LightStone Corp. for their help in refining Fig. 4.

References

- Ambe, D., Kaeriyama, H., Shigenobu, Y., Fujimoto, K., Ono, T., Sawada, H., Saito, H., Miki, S., Setou, T., Morita, T., Watanabe, T., 2014. Five-minute resolved spatial distribution of radiocesium in sea sediment derived from the Fukushima Dai-ichi Nuclear Power Plant. *J. Environ. Radioact.* 138, 264–275.

- Aoyama, M., Hamajima, Y., Hult, M., Uematsu, M., Oka, E., Tsumune, D., Kumamoto, Y., 2016. ^{134}Cs and ^{137}Cs in the North Pacific Ocean derived from the March 2011 TEPCO Fukushima Dai-ichi Nuclear Power Plant accident, Japan. Part one: surface pathway and vertical distributions. *J. Oceanogr.* 72, 53–65.
- Bailly du Bois, P., Laguionie, P., Boust, D., Korsakissok, I., Didier, D., Fiévet, B., 2012. Estimation of marine source-term following Fukushima Dai-ichi accident. *J. Environ. Radioact.* 114, 2–9.
- Belousov, M.P., Gromyko, M.V., Ignatyev, O.V., 2017. Scintillation γ spectrometers for use at nuclear power plants (review). *Instrum. Exp. Tech. (USSR)* 60, 1–19.
- Black, E.E., Buesseler, K.O., 2014. Spatial variability and fate of cesium in coastal sediments near Fukushima, Japan. *Biogeosciences* 11, 5123–5137.
- Buesseler, K., Dai, M., Aoyama, M., Benitez-Nelson, C., Charmasson, S., Higley, K., Maderich, V., Masqué, P., Morris, P.J., Oughton, D., Smith, J.N., 2017. Fukushima Daiichi-derived radionuclides in the ocean: transport, fate, and impacts. *Annu. Rev. Mar. Sci.* 9, 173–203.
- Durrant, C.B., Begg, J.D., Zavarin, M., Kersting, A.B., 2018. Cesium sorption reversibility and kinetics on illite, montmorillonite, and kaolinite. *Sci. Total Environ.* 610–611, 511–520.
- Geological Survey of Japan, 2003. <https://gbank.gsj.jp/geochemmap/ocean/chiho/Tohoku/gazou/TohokuK.gif>.
- Gov. Jpn, 2011. Report of the Japanese government to the IAEA ministerial conference on nuclear safety – the accident at TEPCO's Fukushima nuclear power stations – June 2011. http://japan.kantei.go.jp/kan/topics/201106/iaea_houkokusho_e.html, Accessed date: 25 March 2019.
- Hubbell, J.H., Seltzer, S.M., 1996. X-ray mass attenuation coefficients. <https://physics.nist.gov/PhysRefData/XrayMassCoef/ComTab/water.html>, Accessed date: 25 March 2019.
- IAEA (International Atomic Energy Agency), 2011. Mission report. The Great East Japan Earthquake mission. In: IAEA International Fact Finding Expert Mission of Fukushima Dai-ichi NPP Accident Following the Great East Japan Earthquake and Tsunami, pp. 1–160.
- Kawamura, H., Kobayashi, T., Furuno, A., In, T., Ishikawa, Y., Nakayama, T., Shima, S., Awaji, T., 2011. Preliminary numerical experiments on oceanic dispersion of ^{131}I and ^{137}Cs discharged into the ocean because of the Fukushima Daiichi Nuclear Power Plant disaster. *J. Nucl. Sci. Technol.* 48, 1349–1356.
- Kobayashi, T., Nagai, H., Chino, M., Kawamura, H., 2013. Source term estimation of atmospheric release due to the Fukushima Dai-ichi Nuclear Power Plant accident by atmospheric and oceanic dispersion simulations. *J. Nucl. Sci. Technol.* 50, 255–264.
- Kusakabe, M., Oikawa, S., Takata, H., Misonoo, J., 2013. Spatiotemporal distributions of Fukushima-derived radionuclides in nearby marine surface sediments. *Biogeosciences* 10, 5019–5030.
- Kusakabe, M., Inatomi, N., Takata, H., Ikenoue, T., 2017. Decline in radiocesium in seafloor sediments off Fukushima and nearby prefectures. *J. Oceanogr.* 73, 529–545.
- Matsumoto, A., Myouse, H., Arakawa, H., Higuchi, K., Hirakawa, N., Morioka, Y., Mizuno, T., 2018. The effects of sediment transport on temporal variation in radiocesium concentrations in very shallow water off the southern coast of Fukushima, Japan. *J. Environ. Radioact.* 184–185, 6–13.
- Nakao, A., Ogasawara, S., Sano, O., Ito, T., Yanai, J., 2014. Radiocesium sorption in relation to clay mineralogy of paddy soils in Fukushima, Japan. *Sci. Total Environ.* 468–469, 523–529.
- Nuclear Regulation Authority, Japan, 2014. http://radioactivity.nsr.go.jp/ja/contents/10000/9423/24/report_20140613.pdf (in Japanese). (Accessed: March 25, 2019).
- Nuclear Regulation Authority, Japan, 2015. <http://radioactivity.nsr.go.jp/ja/contents/11000/10925/view.html>. (in Japanese). (Accessed: March 25, 2019).
- Nuclear Regulation Authority, Japan, 2016. <http://radioactivity.nsr.go.jp/ja/contents/13000/12079/view.html>, pp. 62–64 (in Japanese). (Accessed: March 25, 2019).
- Nuclear Regulation Authority, Japan, 2017. <http://radioactivity.nsr.go.jp/ja/contents/14000/13221/view.html>, pp. 4. 2–16–18. (in Japanese). (Accessed: March 25, 2019).
- Nuclear Regulation Authority, Japan, 2018. <http://radioactivity.nsr.go.jp/en/>, Accessed date: 25 March 2019.
- Science Council of Japan, 2014. <http://www.scj.go.jp/ja/info/kohyo/pdf/kohyo-22-h140902-e1.pdf>, Accessed date: 25 March 2019.
- Stohl, A., Seibert, P., Wotawa, G., Arnord, D., Burkhart, J.F., Eckhardt, S., Tapia, C., Vargas, A., Yasunari, T.J., 2012. Xenon-133 and caesium-137 releases into the atmosphere from the Fukushima Dai-ichi nuclear power plant: determination of the source term, atmospheric dispersion, and deposition. *Atmos. Chem. Phys.* 12, 2313–2343.
- Takahashi, Y., Fan, Q., Suga, H., Tanaka, K., Sakaguchi, A., Takeichi, Y., Ono, K., Mase, K., Kato, K., Kanivets, V.V., 2017. Comparison of solid-water partitions of radiocesium in river waters in Fukushima and Chernobyl areas. *Sci. Rep.* 7, 12407.
- Terada, H., Katata, G., Chino, M., Nagai, H., 2012. Atmospheric discharge and dispersion of radionuclides during the Fukushima Dai-ichi Nuclear Power Plant accident, 2; verification of the source term and analysis of regional-scale atmospheric dispersion. *J. Environ. Radioact.* 112, 141–154.
- Thornton, B., Ohnishi, S., Ura, T., Odano, N., Fujita, T., 2013a. Continuous measurement of radionuclide distribution off Fukushima using a towed sea-bed gamma ray spectrometer. *Deep Sea Res.* 179, 10–19.
- Thornton, B., Ohnishi, S., Ura, T., Odano, N., Sasaki, S., Fujita, T., Watanabe, T., Nakata, K., Ono, T., Ambe, D., 2013b. Distribution of local ^{137}Cs anomalies on the seafloor near the Fukushima Dai-ichi Nuclear Power Plant. *Mar. Pollut. Bull.* 74, 344–350.
- Tsumune, D., Tsubono, T., Aoyama, M., Hirose, K., 2012. Distribution of oceanic ^{137}Cs from the Fukushima Dai-ichi Nuclear Power Plant simulated numerically by a regional ocean model. *J. Environ. Radioact.* 111, 100–108.